International Journal of Recent Technology and Engineering (IJRTE)
ISSN: 2277-3878, Volume-8, Issue-1C, May 2019

Numerical and Experimental Investigation of Co-Flow Jet Technique in Clarky-M18 Aerofoil

S Srinivasan, Shreesha M, Tanveer Ahmed, G K Sanjana

Abstract*: The effect of Co-Flow Jet (CFJ) Techniques on the ClarkY-M18 Aerofoil is studied in this paper. The use of Flow Control Techniques (FCT) to enhance the performance of aerofoils has emerged as a prominent area of research in past few decades. CFJ is one of the FCT that adds significant momentum to the boundary layer and delays the boundary layer separation substantially. As a consequence, there is a radical increase in critical Angle of Attack and aerodynamic efficiency of an aerofoil. The drag force is also considerably decreased. Firstly, a numerical analysis is done on three unmodified aerofoils i.e., ClarkY-M18, Eppler 1212 and Wortmann FX66-182. Based on the obtained results, ClarkY-M18 is selected for implementation of CFJ technique. High-pressure air injected tangentially throughout the span at the leading edge while a low-pressure source removes the same amount of air at the trailing edge. The optimum locations and heights of the injection and suction slots is calculated. The desirable sizes of the injection and suction slots are deduced. A numerical study and an experimental investigation are conducted on a full CFJ ClarkY-M18 Aerofoil wing. The results obtained from the experimental and numerical analysis are compared and the augmentation of aerodynamic performance is validated.

Index Terms*: Co-Flow Jet, Delay in Boundary Layer Separation, Flow Control Technique.

Symbols and Acronyms:

$\mathbf{C_L}$, $\mathbf{C_D}$, $\mathbf{C_M}$ lift, drag and moment coefficients
$\mathbf{C_p}$ pressure coefficient
$\mathbf{C_\mu}$ momentum coefficient
D drag
L reference length, lift
m mass flow across the pump
p static pressure
Re Reynolds number,
S planform area
u, v, w velocity components in x, y, z direction
V velocity vector
x, y, z Cartesian coordinates
y+ dimensionless wall normal distance
γ specific heat ratio
μ viscosity
ν kinematic viscosity
ρ fluid density
i, j, k indices
1, 2 subscripts, stands for injection and suction
j subscript, stands for jet
$\mathbf{C_Q}$ Suction Mass Flow Coefficient
∞ free-stream conditions
AoA Angle of Attack
AFC Active Flow Control
CC Circulation Control
CFD Computational Fluid Dynamics
CFJ Co-Flow Jet
DCFJ Discrete Co-Flow Jet
FASIP Flow-Acoustics-Structure Interaction Package
LE Leading Edge
LHS Left Hand Side
M Mach number
OF Obstruction factor
SST Shear-stress transport
TE Trailing edge
ZNMF Zero-net mass flux
VG Vortex generator

Revised Manuscript Received on May 23, 2019.

Srinivasan S Assistant Professor at Department of Aerospace Engineering, RV College of Engineering, Bangalore
Shreesha M pursuing bachelor's degree in Aerospace Engineering at RV college of engineering.
Tanveer Ahmed pursuing Bachelors in Aerospace Engineering at RV College of Engineering, Bengaluru
G K Sanjana student at the Department of Aerospace Engineering, RV College of Engineering, Bangalore

I. INTRODUCTION

Flow control methods and high lift devices are aimed to significantly increase the maximum lift of the wing without increasing its size. The flow control methods described in this research are based on the boundary layer principles first described by Prandtl in 1904 [10]. When an adverse pressure gradient acts on a flow, the boundary layer size increases and the boundary layer velocity directly above the wall decreases (the velocity at the wall remain zero because of the no-slip condition). If the adverse pressure gradient increases, the boundary layer velocity direction changes and the boundary layer separates. This local phenomenon is accompanied with the creation of large vortices, an increase of the drag and a decrease of the lift, which is known as stall. Alternately, a thin boundary layer with reasonably large momentum can sustain a large adverse pressure gradient before it detaches. This understanding led to the current era of aerofoil design where boundary layer control method plays an important role.

The vortex generators, flaps and slats are called passive flow control because no external source of energy is supplied. In the passive flow control method, the energy is transferred from the main flow to the boundary layer. Conversely, the active flow control method requires an external source of energy. For active flow control, the energy is transferred from this external source of energy (pump, aircraft compressor, plasma discharge etc.) to the fluid. Due to their intrinsic complexity, active flow control methods are not as common as

Retrieval Number: A10470581C19/19©BEIESP
Published By:
Blue Eyes Intelligence Engineering
& Sciences Publication

their passive counterparts. Nonetheless the recent research presented below show their enormous potential.

Vortex generators (VGs) are among the most common flow control methods because of their ease of implementation and effectiveness. VGs improve performance and control authority at low airspeed and high AoA by generating vortex structures that transfer energy from the main flow into the boundary layer. More recently, Barrett et al. studied experimentally an intelligent vortex generator that deploys close to the stall AoA and conforms to the wing otherwise [13]. Slats and flaps are also common lift enhancing systems used in aviation and are used to shorten take-off and landing distances. The deployment of flaps and slats increases the camber and, in most cases, the planform area of the wing. Thereby the lift increases at the expense of a higher drag and moment. The first flap to be implemented on an actual aircraft was the plain flap. Despite of its modest aerodynamic efficiency, the plain flap is still common today because of its simplicity. However, in order to increase effectiveness and efficiency, the slotted flap was constructed with a gap between the wing and the flap. Harris et al. studied a variety of NACA aerofoils equipped a single slotted flap [15] and a 30% chord double slotted flap [16]. Modern wing designs often combine various slats and flaps elements. Morgan Jr. (1981) studied experimentally such a wing [19]. The combination of slats and flaps shifted the C_L vs AoA curve upward by as much as 1.5.

Shortly after writing the first description of the boundary layer concept in 1904 [9], Prandtl successfully delayed the flow separation on a circular cylinder by sucking in the low energy fluid in the boundary layer. The effect of boundary layer suction on a wing performance was studied as early as 1935 by Schrenk in [20]. Two geometries were studied, a 40% thickness ratio wing with various suction slot positions and widths and a 20% thickness ratio wing with a suction slot located close to the trailing edge flap. The thick wing performance is very poor without suction. However, a small suction mass flow coefficient C_Q of 0.0022 is sufficient to keep the flow attached up to AoA = 20°. In a pitching aerofoil experimental investigation, Muller-Vahl et al. recorded the effect of continuous blowing on a NACA 0018 aerofoil from the leading edge and at mid-chord slots [24]. He focused on the dynamic stall of the aerofoil as it oscillates between −2.5° and 32.5°. The dynamic stall mitigation obtained by leading edge blowing yielded an average lift increase and the mid-chord blowing was able to remove the trailing edge separation but not the leading-edge separation. Plasma flow control method is a recent technique in which a dielectric barrier discharge ionizes the surrounding flow. Post et al. (2004) studied experimentally the separation control of a generic aerofoil using plasma actuators to generate a steady wall jet in the direction of the flow [26]. The plasma actuators delayed the stall AoA by up to 8° and the resulting maximum C_L is increased from about 0.55 to 0.75. The drag is lower for AoAs past the stall AoA of the unexcited aerofoil. The circulation control (CC) aerofoil [27] relies on the Coanda effect, which creates a favourable pressure gradient on a curved surface to prevent flow separation. Traub et al. studied the performance of a self-contained CC wing with the pump located inside a S8036 aerofoil [28]. The maximum lift coefficient is increased by 39% from 0.848 to 1.176. The added power consumption of the pump and the relatively high drag of the CC wing means that the CC wing energy efficiency is fairly low.

To overcome the disadvantages of the above methods, Zha and his team [29], [30] developed a novel concept of active flow control aerofoil using co-flow jet, which radically augments the lift, reduces drag, and increases the stall AoA at low energy expenditure. This study aims to demonstrate the effectiveness of a CFJ aerofoil with discrete injection and suction slots in the following aspects-

1. Lift augmentation
2. Stall margin increase
3. Drag reduction

In this paper, prior to the numerical and experimental investigation, sub-studies of different baseline aerofoils are performed. A suitable aerofoil is selected, on which the CFJ study will be performed. The ideal configuration of the full CFJ injection and suction slots is obtained and, the numerical and experimental studies are conducted on it.

II. METHODOLOGY

The CFJ aerofoil concept is illustrated below. The aerofoil suction surface is modified with an injection slot near the LE and a suction slot near the TE. A small mass flow is withdrawn into the aerofoil suction slot, pressurized by a pumping system inside the aerofoil, and re-injected through the injection slot tangentially to the main flow. The whole process does not add any mass flow to the system and hence is a zero-net mass flux flow control and the energy loss are minimized.

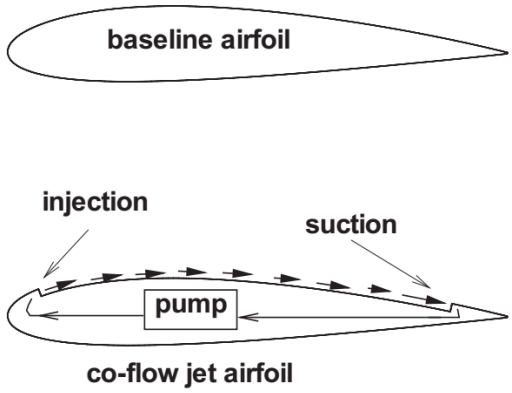

Fig 1: Implementation of CFJ on a generic aerofoil [4]

2-D Numerical study is performed on three different unmodified aerofoils and the results are compared to select a suitable aerofoil for CFJ study. Stream conditions like Reynolds number and Mach number are foreordained based on literature survey and available wind tunnel equipment. 2-D Numerical CFJ studies will be conducted for the desired value of C_μ. Required compressor pressure and the vacuum suction pressure will be determined by repeating the analysis for different pressure values until the mass flow rates at the injection and the suction slots are within 5% of each other. Grid-independent study is performed by refining the mesh to obtain a reliable solution. The unmodified and the CFJ wings are fabricated using precision machining techniques, including CNC and 3D-printing. Experimental validation is carried out on both the aerofoils considering flow conditions similar to that of numerical analysis.

In numerical analysis, the software used for designing, meshing, processing and post processing:

- Designing - CATIA (Computer Aided Three-Dimensional Interactive Application)
- Meshing - Pointwise V17.2
- Solver - ANSYS Fluent 15.0
- Post-processing - Tecplot 360

Retrieval Number: A10470581C19/19©BEIESP
Published By:
Blue Eyes Intelligence Engineering
& Sciences Publication

III. UNMODIFIED AEROFOIL - NUMERICAL ANALYSIS

A. Candidate aerofoils

The following aerofoils were subjected to numerical studies –

1. *ClarkY-M18* - Maximum thickness 18% at 29.6% chord and maximum camber 3.6% at 39.6% chord (Fig 2).
2. *Eppler 1212* - Maximum thickness 17.7% at 23.4% chord and maximum camber 3.2% at 36.4% chord (Fig 3).
3. *Wortmann FX66-182* - Maximum thickness 18.2% at 33.9% chord and maximum camber 3.8% at 37.1% chord (Fig 4).

Fig 2: ClarkY-M18 shape

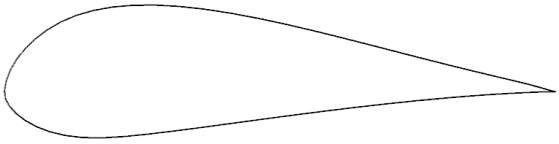

Fig 3: Eppler 1212 shape

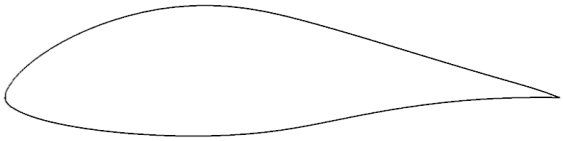

Fig 4: Wortmann FX66-182 shape

B. Aerofoil geometry and free stream conditions

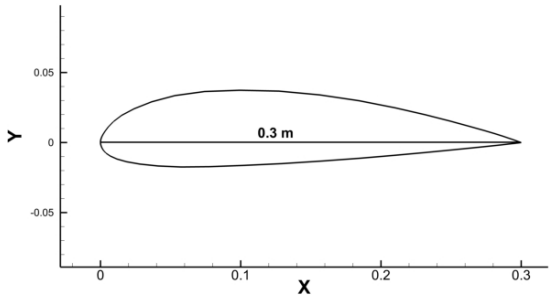

Fig 5: Geometry of ClarkY-M18 baseline aerofoil

The free-stream Mach number was taken as 0.03 since it would require lower compressor and suction pressures to maintain the net-mass flux at zero. The optimum Reynolds number range for the considered aerofoils was between 200,000 and 250,000. Hence, we considered a chord of 0.3 m, thus yielding a Re of 200,000.

Fig 5 shows the geometry for the ClarkY-M18 baseline aerofoil. The other aerofoils were similarly designed. The geometry was designed in CATIA V5 Drafting.

C. Mesh

The original 2D mesh was constructed using the C-mesh topology (Fig 7). A total of 213 points were placed around aerofoil, 50 points on suction surface, 50 points on the pressure surface and 113 points normal to the aerofoil. The total mesh size was 12656 cells. The far-field boundary was located 15 chords away from the aerofoil. To resolve the turbulent boundary layer, the first grid point is placed at y+ ≈ 1. A mesh quality analysis of the Clark-M18 mesh yielded a max skewness of 0.13, indicating a high-quality mesh. The other aerofoils underwent a similar meshing process.

To obtain a trustworthy solution, it is important to have a grid independent study of the flow (Fig 8). This is commonly achieved by refining the overall grid and/or by extending the far-field. Since the far-field distance was already quite large, the existing mesh was refined to obtain a mesh with 35,600 cells (*three* times the original). The mesh quality was also improved. The maximum skewness reduced to 0.095 and the minimum orthogonality was 88%.

D. Boundary conditions

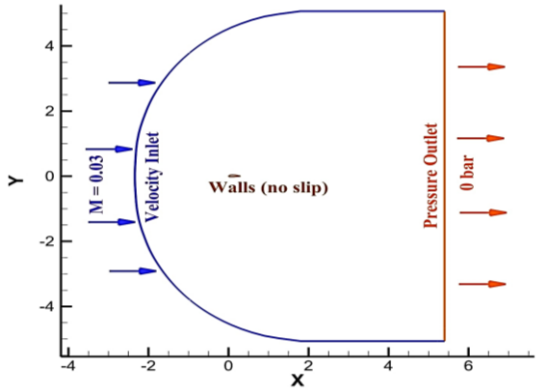

Fig 6: Boundary conditions for baseline aerofoil

The free-stream Mach number was maintained at 0.03 throughout the analysis (Fig 6). For standard sea-level conditions, this yields a free-stream velocity of 10.3 m/s. The angle of inclination of the inlet velocity vector with respect to the chord line was varied to be equal to the angle of attack (AoA) in consideration. The far-field pressure outlet was maintained at 0 bar to simulate ambient conditions. Air density, ambient pressure and dynamic viscosity were taken corresponding to standard sea-level conditions. The aerofoil surface was, of course, assigned a no-slip wall condition.

E. Solution Setup

The Pressure based Navier-Stokes (PBNS) Equations, coupled with a Semi-Implicit Pressure Linked Equation (SIMPLE) scheme was used to solve the flow-field problem. Turbulence modelling had to be carried out since the flow was viscous and non-laminar. The SST k-ω model was utilized since it is a proven model. Second order spatial discretization was carried out to further improve the accuracy of the solution.

F. Results

After obtaining sufficient convergence in numerous solution monitors (continuity equations, lift, drag, moments), the solution files were transferred to the post-processing software (Tecplot 360) and processed.

1. ClarkY-M18

At an AoA of -3.5°, we see that there is very little pressure difference between the top and bottom surfaces

Retrieval Number: A10470581C19/19©BEIESP
Published By:
Blue Eyes Intelligence Engineering
& Sciences Publication

(Fig 9). This creates almost *zero* lift on the aerofoil. Thus, for

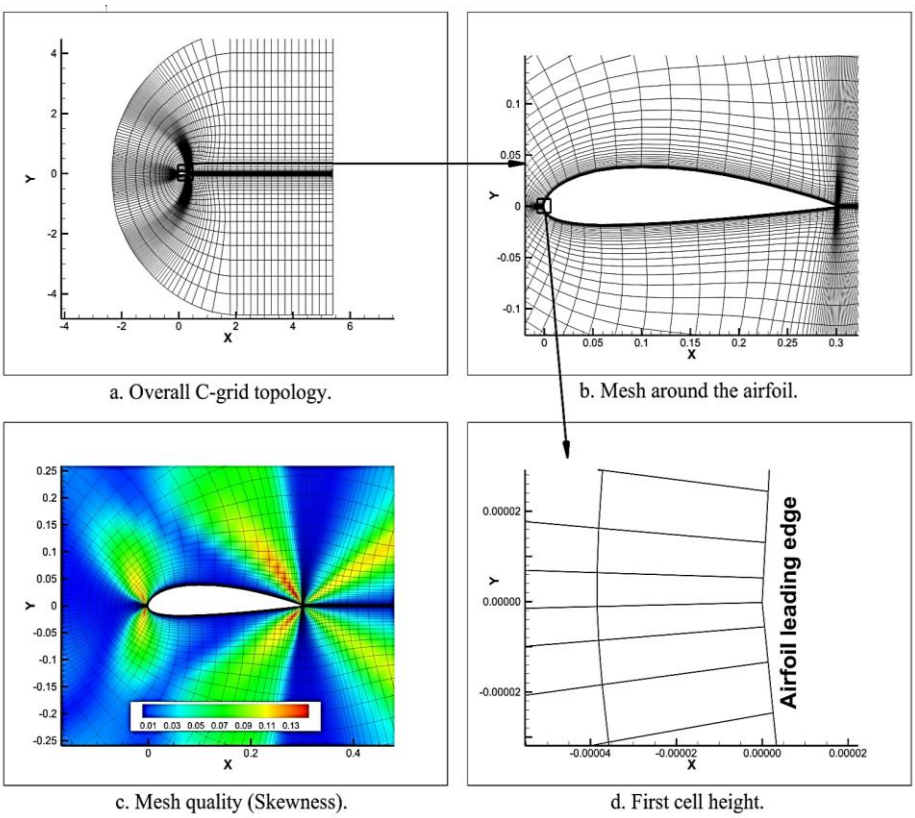

a. Overall C-grid topology.
b. Mesh around the airfoil.
c. Mesh quality (Skewness).
d. First cell height.

Fig 7: Original clarky-M18 C-mesh topology with zoomed in views of the aerofoil and the leading edge, along with mesh quality analysis

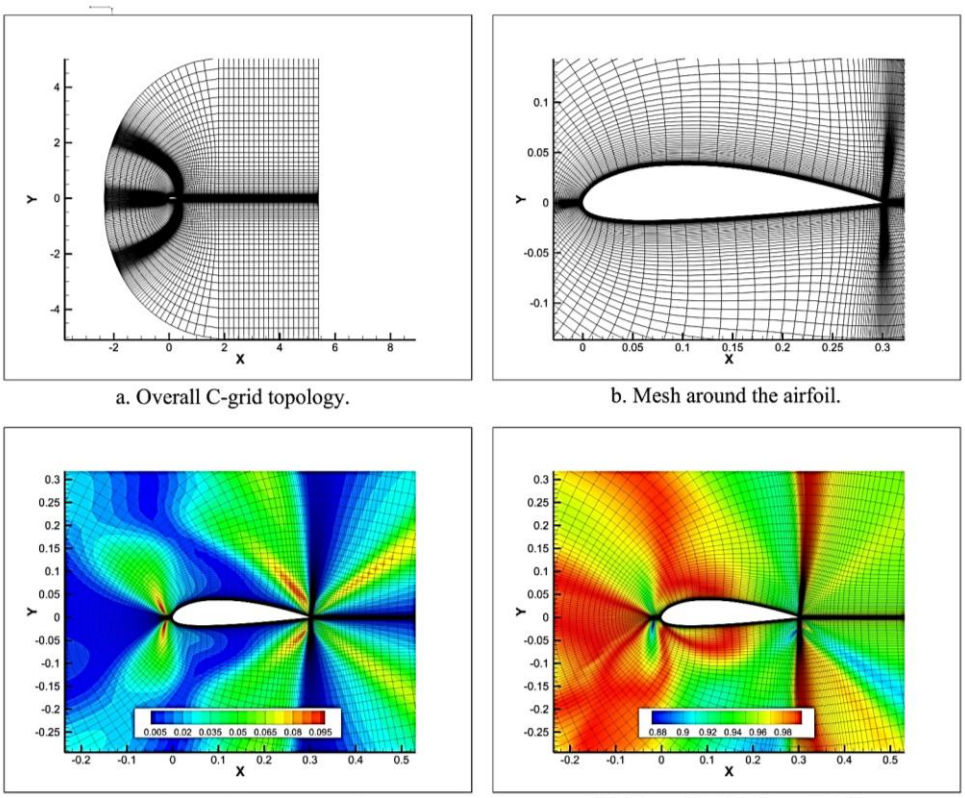

a. Overall C-grid topology.
b. Mesh around the airfoil.
c. Mesh quality (Skewness).
d. Mesh quality (Orthogonality).

Fig 8: Refined clarky-M18 C-mesh topology with mesh quality analysis

this aerofoil, the zero-lift line is inclined at -3.5° to the chord line. Thus, $\alpha_{L=0}$ = -3.5°

At an AoA of 0°, we see a noticeable pressure

Retrieval Number: A10470581C19/19©BEIESP

Published By:
Blue Eyes Intelligence Engineering
& Sciences Publication

difference between the upper and lower surface of the aerofoil (Fig 10). Thus, positive lift is generated at this AoA. In other words, $C_{L,0}$=0.2308.

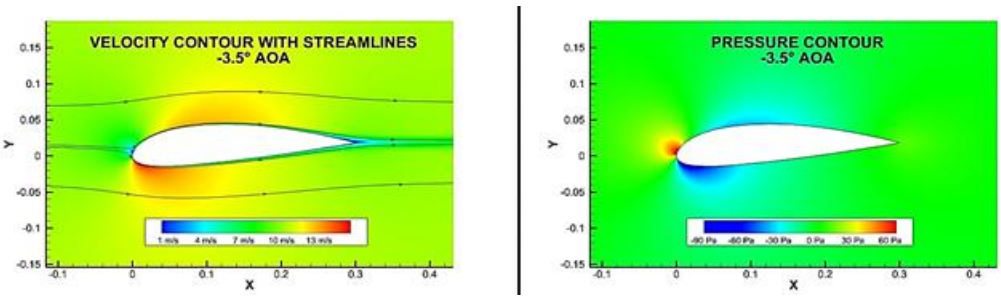

Fig 9: Velocity and Pressure contours for -3.5° AoA

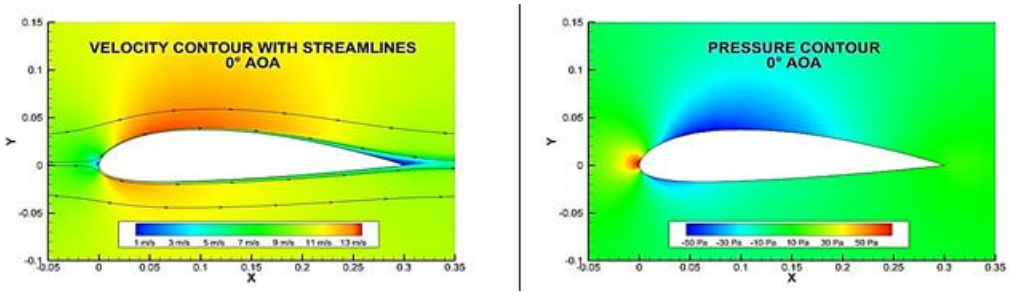

Fig 10: Velocity and Pressure contours for 0° AoA

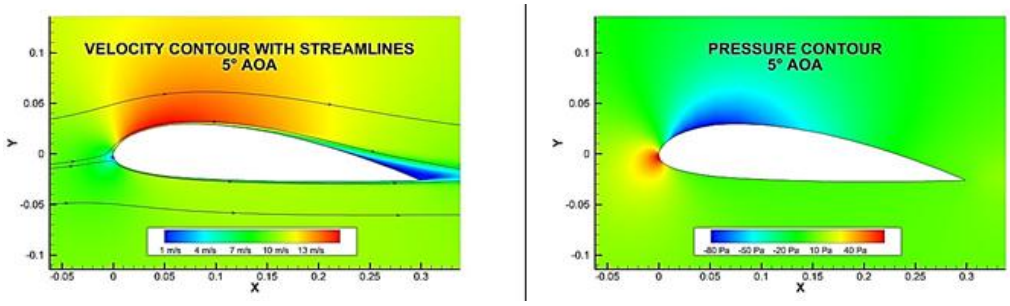

Fig 11: Velocity and Pressure contours for 5° AoA

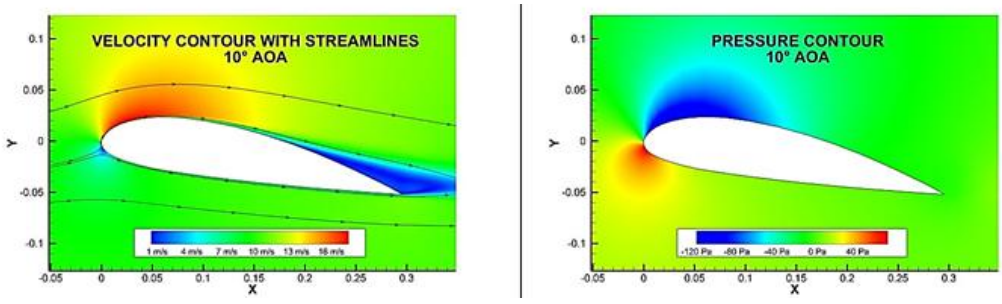

Fig 12: Velocity and Pressure contours for 10° AoA

At an AoA of 5°, there is a significant pressure difference between the upper and lower surface of the aerofoil (Fig 11). The lift on the aerofoil thus increases. The flow separates at approximately 20% of the chord length before the trailing edge, on the upper surface. Also, the maximum value of *L/D* occurs at this AoA.

At an AoA of 10°, The flow separates at approximately 35% of the chord length before the trailing edge, on the upper surface (Fig 12). We can expect stall to occur within the next 5°.

At an AoA of 14°, the lift reaches its peak value ($C_{L\,\max}$ = 1.214) (Fig 13). The flow separates at approximately 50% of the chord length. This is the stalling AoA for this aerofoil. After this AoA, we can expect a decrease in lift and significant drag increase.

At an AoA of 16°, the lift decreases, since the aerofoil has already stalled. The flow separates at approximately 63% of the chord length (Fig 14). Due to large eddies being created in the wake region; the drag increases rapidly. Similar results were obtained for other aerofoils and the obtained results are assembled in form of graphs and tables.

Retrieval Number: A10470581C19/19©BEIESP

Published By:
Blue Eyes Intelligence Engineering
& Sciences Publication

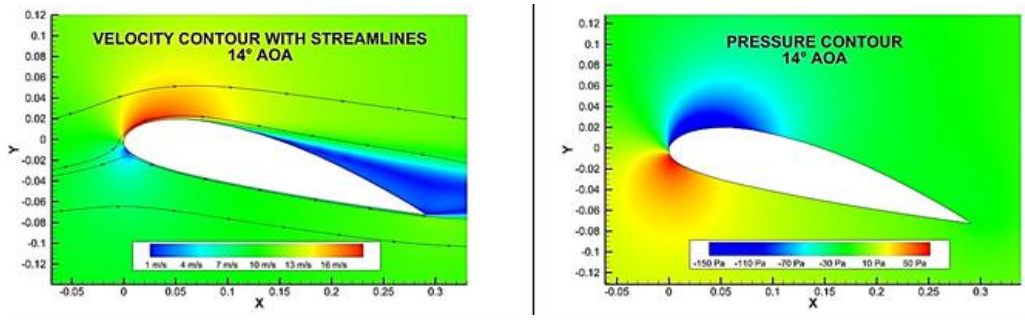

Fig 13: Velocity and Pressure contours for 14° AoA

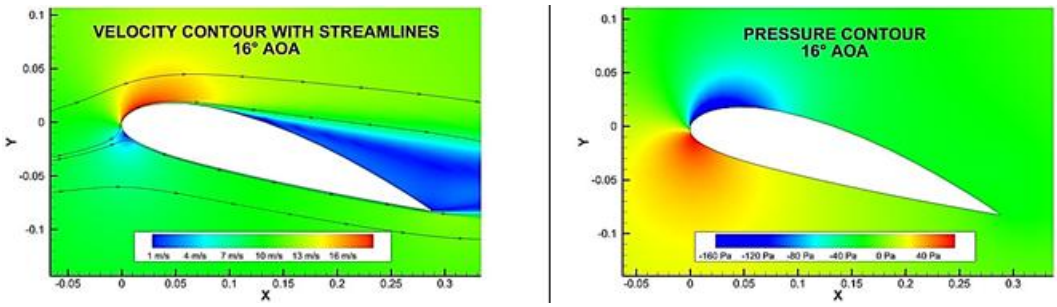

Fig 14: Velocity and Pressure contours for 16° AoA

G.Assembled results

1. ClarkY-M18

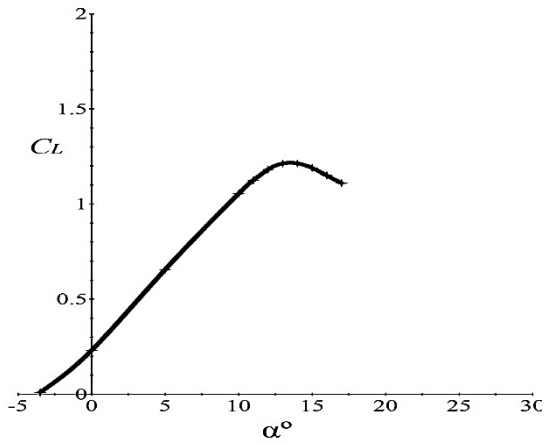

Fig 15: ClarkY-M18: CL v/s AoA

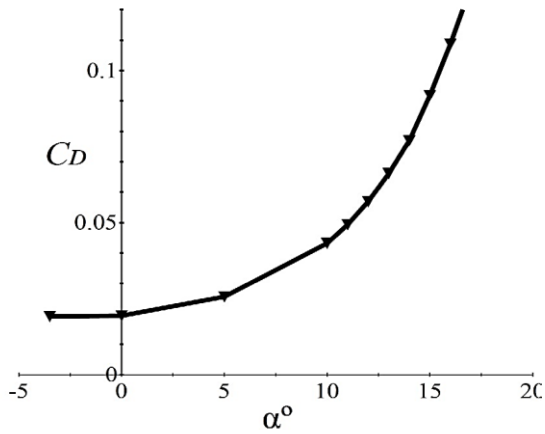

Fig 16: ClarkY-M18: CD v/s AoA

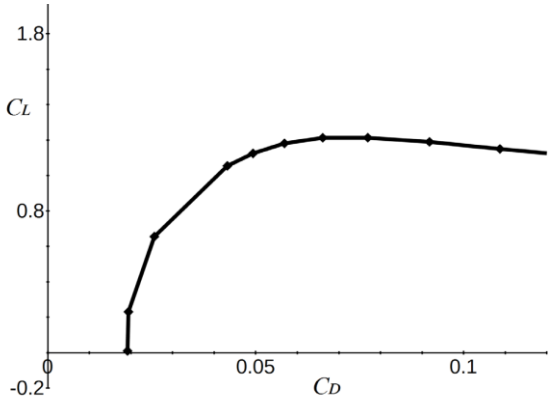

Fig 17: ClarkY-M18: CL v/s CD

Table I: ClarkY-M18: result table

α°	CL	CD	CL/CD
3.5	0.00980	0.01920	0.51042
0	0.23080	0.01940	11.89691
5	0.65530	0.02560	**25.59766**
10	1.05440	0.04320	24.40741
11	1.12500	0.04940	22.77328
12	1.18160	0.05690	20.76626
13	1.21350	0.06610	18.35855
14	1.21310	0.07700	15.75455
15	1.17020	0.09180	12.74728
16	1.10130	0.10870	10.13155
17	0.98530	0.12750	7.72784

Retrieval Number: A10470581C19/19©BEIESP

Published By:
Blue Eyes Intelligence Engineering
& Sciences Publication

2. Eppler 1212

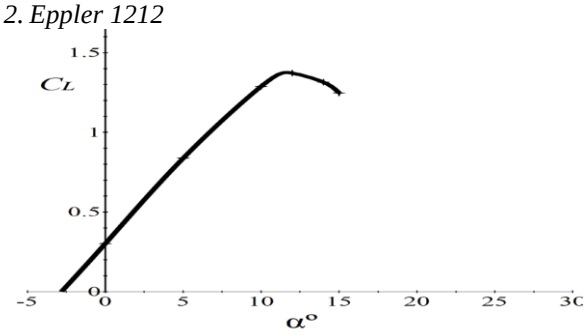

Fig 18: Eppler 1212: CL v/s AoA

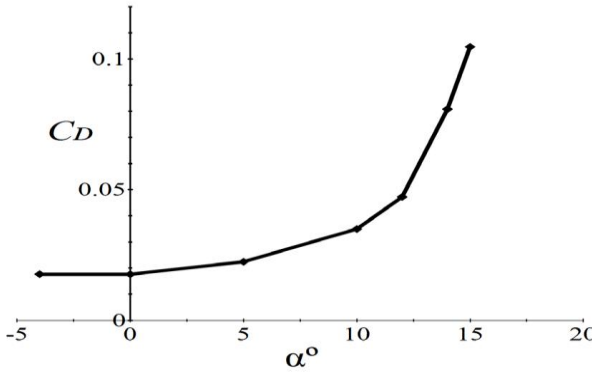

Fig 19: Eppler 1212: CD v/s AoA

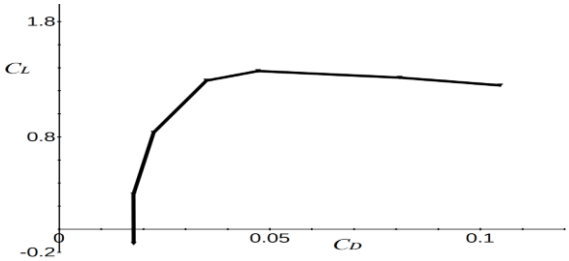

Fig 20: Eppler 1212: CL v/s CD

Table II: Eppler 1212: result table

α°	CL	CD	CL/CD
-4	-0.12390	0.01770	-7.00000
-3	-0.01540	0.01730	-0.89017
0	0.30180	0.01760	17.14773
5	0.83780	0.02240	**37.40179**
10	1.28800	0.03490	36.90544
12	1.37140	0.04720	29.05508
14	1.31430	0.08080	16.26609
15	1.24680	0.10470	11.90831

3. Wortmann FX66-182

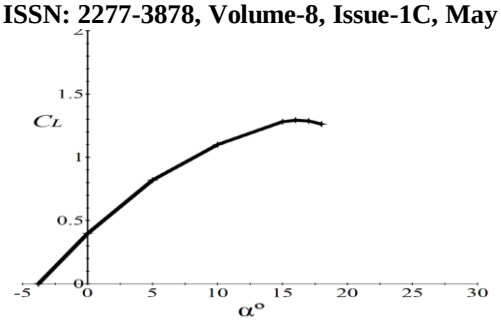

Fig 21: FX66-182: CL v/s AoA

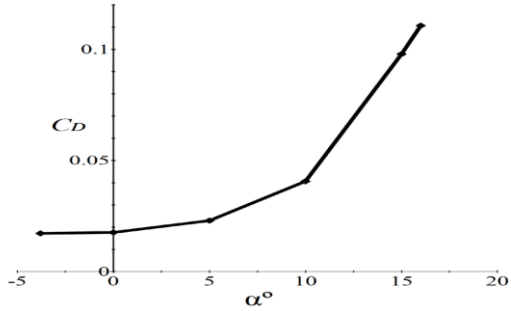

Fig 22: FX66-182: CD v/s AoA

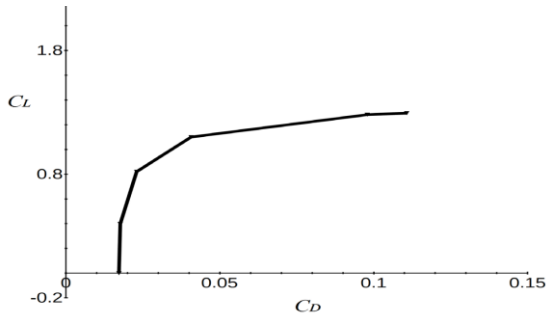

Fig 23: FX66-182: CL v/s CD

IV. AEROFOIL SELECTION

The *ClarkY-M18* was chosen as the baseline aerofoil on which the CFJ modification would be done. The reasons to do so are explained below.

Firstly, the ClarkY-M18 has a thicker section towards the trailing edge. This makes it easier to install suction slots with minimal structural problems.

The other two aerofoils have comparatively thinner sections near the trailing edge. The addition of a suction slot will weaken the trailing edge portion and might lead to cracks or breakage.

Retrieval Number: A10470581C19/19©BEIESP

Published By:
Blue Eyes Intelligence Engineering
& Sciences Publication

Table III: FX66-182: result table

α°	CL	CD	CL/CD
-3.8	0.00120	0.01720	0.06977
0	0.39850	0.01760	22.64205
5	0.81990	0.02290	**35.80349**
10	1.10020	0.04070	27.03194
15	1.28100	0.09790	13.08478
16	1.29310	0.11070	11.68112
17	1.28710	0.12460	10.32986
18	1.26210	0.14490	8.71015

Secondly, the ClarkY-M18 has noticeably poorer performance than the other two aerofoils, in terms of lift generation and drag. This can be inferred from the numerical investigation. It will be interesting to see whether the CFJ modification will make it perform better than the other two aerofoils.

Thirdly, the aerofoil is very popular, being used extensively in R/C-models, UAVs and small-scale airplanes. The results generated for the CFJ modification done on this aerofoil can be directly compared with in-flight experimental data in the future.

V.CO FLOW JET AEROFOIL - NUMERICAL ANALYSIS

Numerical investigation is performed on modified co-flow jet ClarkY-M18 aerofoil.

A.Aerofoil geometry

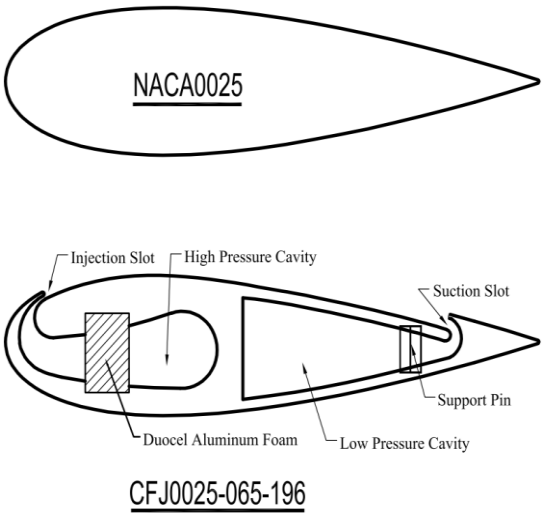

Fig 24: Typical CFJ aerofoil

Injection and Suction slot heights:

The size of the injection and the suction slots must be such that it must not choke the flow at the maximum expected mass flow rate.

We know that the momentum coefficient $C\mu$ is given by-

$$C\mu = \frac{\dot{m}V_j}{\frac{1}{2}\rho V_\infty^2 S} \quad (1)$$

A constant C_μ value of 0.05 was considered based on the capacity of the compressor available for experiment. The literature [4] showed that the minimum velocity of the injected flow must be at least twice the free-stream velocity to obtain excellent CFJ performance.

$$V_{jet,min} = 2 * V_\infty \quad (2)$$

Mass flow rate is given by,

$$\dot{m} = \rho A V \quad (3)$$

Substituting ρ as 1.225, V_∞ as 10.3 m/s and reference area S as 0.3 m^2, we obtain the value of maximum expected mass flow rate from as $\dot{m}_{max}$ = 0.046 kg/s.

Maximum mass flow rate = mass flow rate of jet

$$\dot{m} = \rho * A(jet) * V(jet) \quad (4)$$

Substituting $\dot{m}$ = 0.046 kg/s and $V_{(jet)}$ as 20.6 m/s, we get area of jet as 0.0019 m^2.

$$A_{inj} = span * h_{inj} \quad (5)$$

For a span of 1 m, the slot height is obtained as h_{inj} = 1.9 mm. This is equal to 0.63% of the chord. Thus, the injection slot height is dervish.

To obtain the suction slot height, we have to consider the fact that the vacuum pressure required in the suction cavity must be reduced (to reduce power consumption). The suction slot height having a value twice that of the injection slot was found to be the most suitable. Thus, the suction slot height was taken as 1.3% of the chord.

Injection and suction slot locations:

The static pressure is lower towards the front on the aerofoil top surface. Lesser injection pressure is required to produce the same jet velocity. Hence the most upstream location is desired for placing the injection slot. But due to practical concerns (slot strength and rigidity, allowance for machining), the injection slot could only be pushed forward to 7% of the chord from the leading edge.

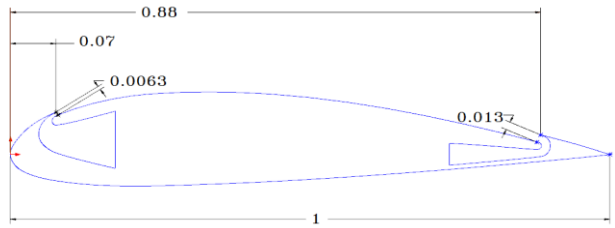

Fig 25: CFJ clarky-M18-063-130

The suction slot, on the other hand must be placed at the most downstream location possible if aerodynamic efficiency is required. This is because the aerofoil with the more downstream location generates higher lift and lower drag. The longer jet has more space to mix an energize the flow and increases the circulation. This, however, occurs at the expense of higher energy consumption.

Retrieval Number: A10470581C19/19©BEIESP
Published By:
Blue Eyes Intelligence Engineering
& Sciences Publication

The final geometry is shown in Fig 25. The dimensions are normalized with respect to a unit chord

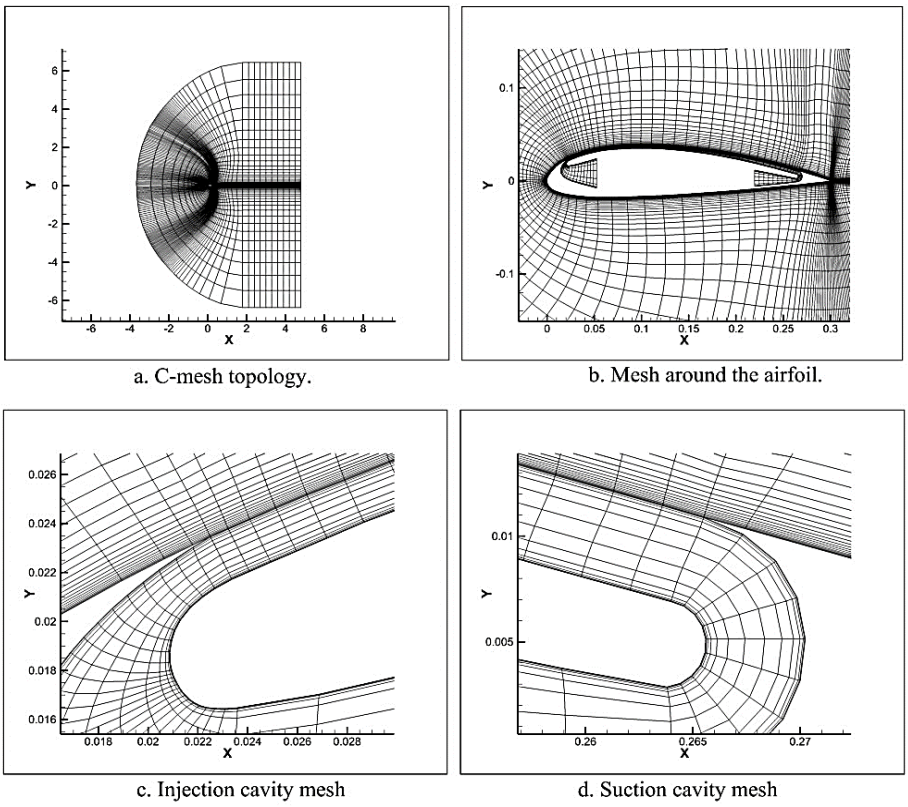

Fig 26: Original mesh around CFJ aerofoil

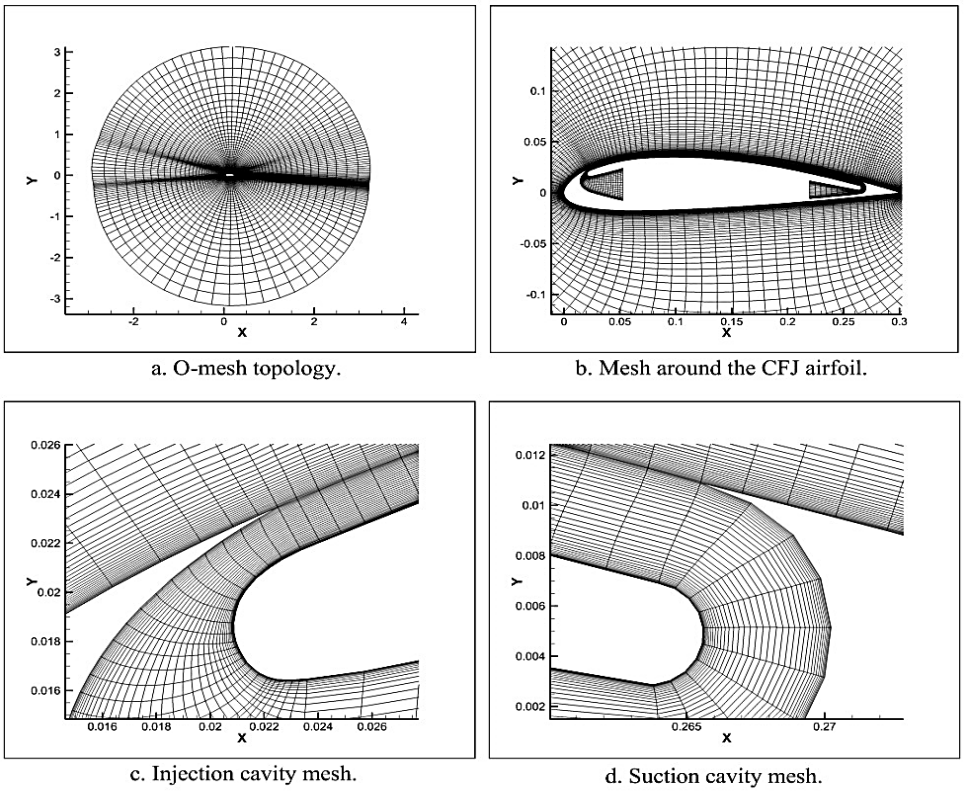

Fig 27: O-mesh around the CFJ aerofoil

length. The internal cavity geometries were finalized after a few test simulations with different shapes. The cavities mush be aerodynamically smooth with little to no pressure losses associated with them.

Following Zha's naming convention [25], [30] CFJ xxxx-inj-suc, the aerofoil is named as CFJ ClarkY-M18-063-130 (Fig 25).

Retrieval Number: A10470581C19/19©BEIESP

Published By:
Blue Eyes Intelligence Engineering
& Sciences Publication

B. Mesh

The original 2D mesh was constructed using the C-mesh topology (Fig 26). A total of 297 points were placed around aerofoil, 63 points on the top surface, 50 points on the bottom, 33 points for the injection cavity walls, 19 points for the suction cavity walls, 15 points for the slot edges and 117 points normal to the aerofoil. The total mesh size was 13368 cells. The far-field boundary was located 15 chords away from the aerofoil. To resolve the turbulent boundary layer, the first grid point is placed at $y+ \approx 1$.

To have a grid independent study of the flow, a mesh with an O-topology was generated with 22,525 cells (Fig 27).

The mesh quality analysis shows a maximum skewness of 0.28, with an average value of 0.04 which is an indication of a high-quality mesh. The highly skewed cells are four in number and are located at the trailing edge of the aerofoil, due to the sharp contour of the trailing edge.

C. Boundary conditions

Apart from the boundary conditions applied for unmodified aerofoil, additional boundary conditions were imposed to conduct the analysis of the CFJ aerofoil (Fig 28). An inlet, with total pressure specified, was used for incoming flow in the injection cavity. An outlet, with fixed suction static pressure, was defined for the outflow in the suction cavity. The walls of the cavities were assigned a wall no-slip boundary condition.

D. Solution setup

The Pressure based Navier-Stokes (PBNS) Equations, coupled with Semi-Implicit Pressure Linked Equation (SIMPLE) scheme was used to solve the flow-field problem. Similar to before, the SST k-ω model was utilized. Second order spatial discretization was carried out to further improve the accuracy of the solution.

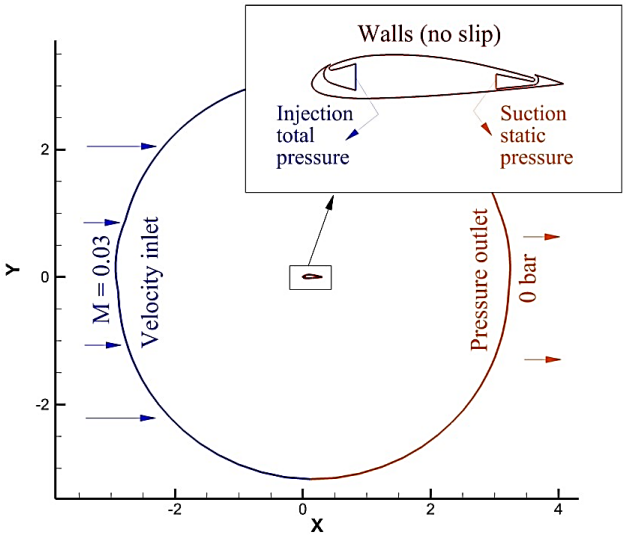

Fig 28: Boundary conditions for CFJ aerofoil

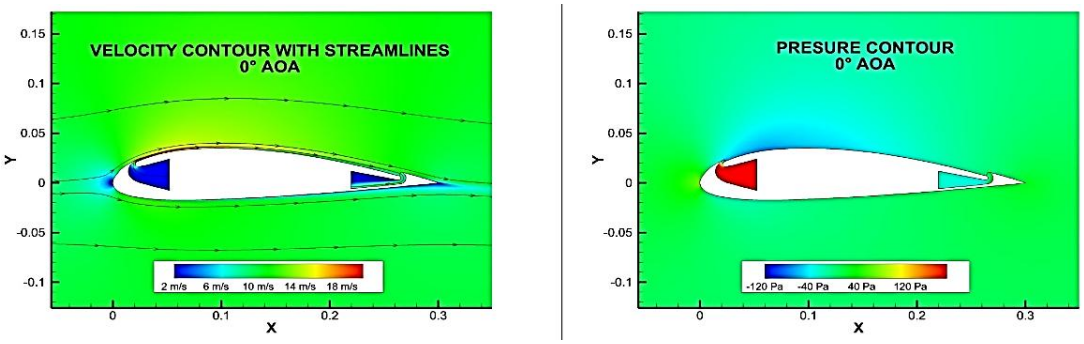

Fig 29: Velocity and Pressure contours for 0° AoA

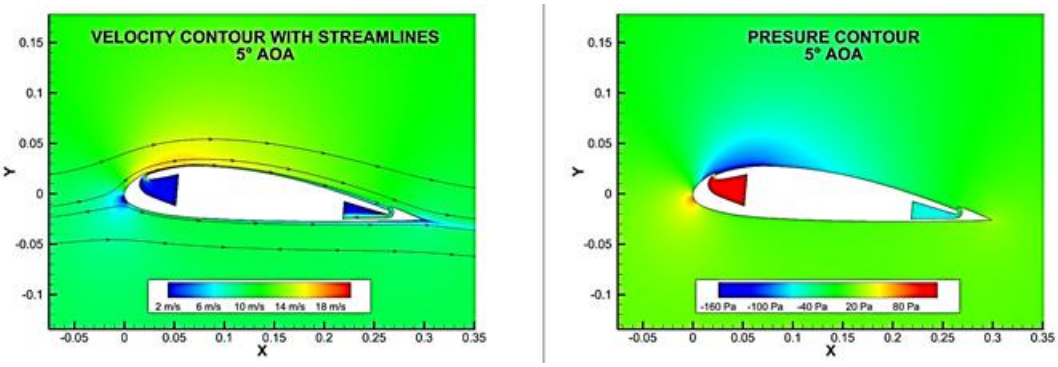

Fig 30: Velocity and Pressure contours for 5° AoA

E. Results

At an AoA of 0°, significant circulation is established around the aerofoil (Fig 29). Thus, additional lift is generated at this AoA. In other words, for the CFJ aerofoil, $C_{L,0}$=0.5880. Also, the magnitude of the eddy vortices downstream of the aerofoil is decreased, resulting in negative drag (thrust) being produced.

At an AoA of 5°, the combination of the enhanced circulation and the lowered

Retrieval Number: A10470581C19/19©BEIESP

Published By:
Blue Eyes Intelligence Engineering
& Sciences Publication

pressure on the top surface leads to substantial lift generation (Fig 30). There is no indication of any flow separation over the aerofoil surface. At an AoA of 10°, the flow just starts to separate at the trailing edge (Fig 31).

The lift generated is up to 40% more than that generated by the baseline at this AoA. At an AoA of 15°, the static pressure at the suction cavity required to maintain the zero net mass flux condition starts decreasing drastically (increase in vacuum pressure) (Fig 32). The drag is at a low positive value.

At an AoA of 20°, the aerofoil has stalled since the detrimental effects of the jet force on the lift becomes so string that it results in overall lift reduction (Fig 33).

The comparative studies of the lift, drag and aerodynamic efficiency generated in baseline and the CFJ modification are shown (Fig 34 - 36).

The maximum value of C_L has increased by 0.45, from 1.214 for the baseline case to 1.6623 for the CFJ case. The stall angle has also shifted by 3 degrees in favour of the CFJ aerofoil. Up to an AoA of 15°, the aerofoil generates negative drag (thrust). The aerodynamic efficiency of the aerofoil is, as expected, much better in the case of CFJ modification.

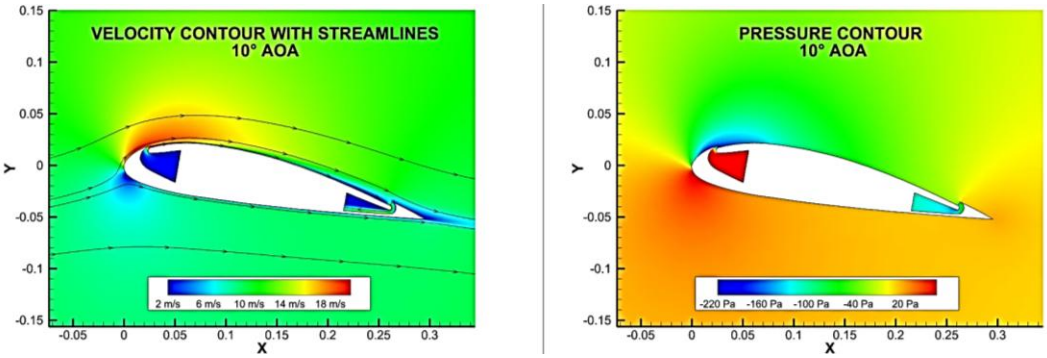

Fig 31: Velocity and Pressure contours for 10° AoA

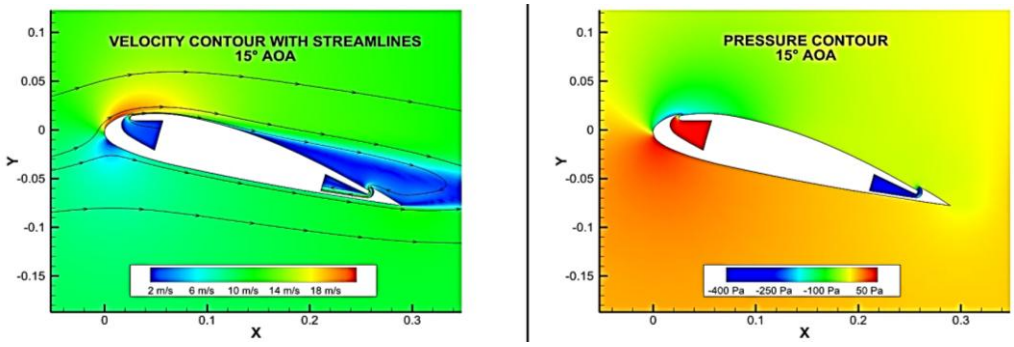

Fig 32: Velocity and Pressure contours for 15° AoA

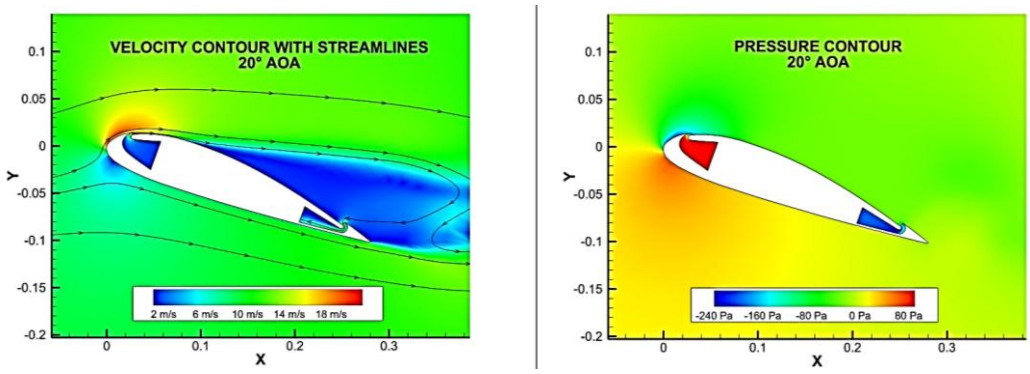

Fig 33: Velocity and Pressure contours for 20° AoA

Retrieval Number: A10470581C19/19©BEIESP
Published By:
Blue Eyes Intelligence Engineering
& Sciences Publication

Table IV: Results Table

$\alpha°$	$C\mu$	$P_{0,inj}(Pa)$	$P_{s,suc}(Pa)$	$\dot{m}_{inj}$ (kg/s)	V_{jet} (m/s)	CL	CD	CL/CD
0	0.0504	198	-33	0.045	21.750	0.588	-0.197	-2.98477
5	0.0502	143	-79	0.045	21.740	1.170	-0.156	-7.49808
10	0.0503	81	-162	0.045	21.720	1.586	-0.093	-17.0344
15	0.0501	66	-219	0.045	21.710	1.655	0.008	197.0357
16	0.0502	64	-231	0.045	21.730	1.662	0.031	53.79612
17	0.0500	61	-243	0.045	21.710	1.632	0.071	23.01975
20	0.0501	58	-275	0.045	21.710	1.497	0.168	8.921931

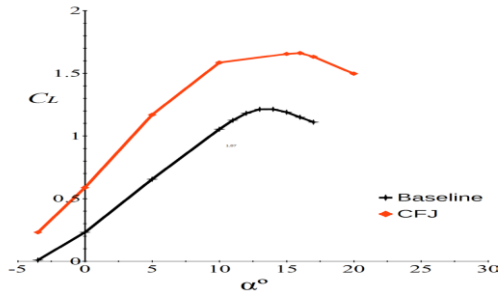

Fig 34: CL v/s AoA comparison

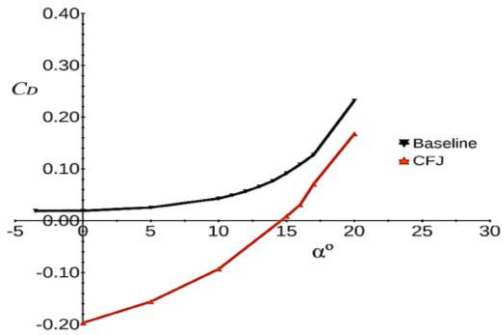

Fig 35: CD v/s AoA comparison

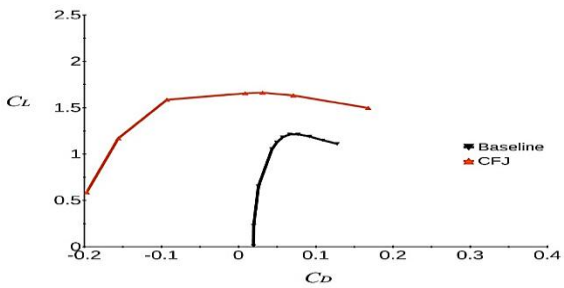

Fig 36: CL v/s CD comparison

VI. CO FLOW JET AEROFOIL - EXPERIMENTAL VALIDATION

A. Design considerations

The external geometry of the CFJ aerofoil was finalized during numerical Analysis. The shapes of the interior cavities were driven by three factors:

- The minimum area required for flow without being choked
- Internal aerodynamic characteristics
- Ease of machining

Since air will be supplied to and removed from the aerofoil to create the co-flow jet, the internal cavities needed to have large enough areas so that there would be no choked flow and the mass flow rates could be controlled for various tests. The calculation is same as presented in numerical analysis.

The internal features should include aerodynamic shapes for the most effective use of high-pressure air to generate the jet. This was done by ensuring that there were no jagged corners or abrupt turning of the flows. Also, it was ensured that the co-flow enters and exits the cavities in a direction tangential to the local free-stream. The internal cavity geometry was also finalized during the numerical analysis stage.

Throughout the design of the model, manufacturing capabilities were considered to ensure that the final aerofoil would be easy to machine without complicated and costly features. The thin edges at the injection and suction slots were made to a thickness within reason, leaving enough material to withstand the pressures maintained in the cavities.

B. Final Design

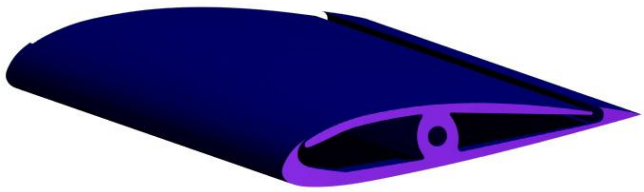

Fig 37: Trimetric of the CFJ aerofoil

The CFJ wing was designed in CATIA V5 Product Design module. The final design iteration is shown (Fig 37– 38). The chord and the span are 0.3 m and 0.6 m respectively. A central hole was provided to fit a tube of 0.017 m diameter. The purpose of this tube is to help in setting the AoA for the aerofoil. A provision is made in the injection cavity to install a flow straightener along the span. The compressor and vacuum pump air connection system is shown (Fig 39).

Retrieval Number: A10470581C19/19©BEIESP

Published By:
Blue Eyes Intelligence Engineering
& Sciences Publication

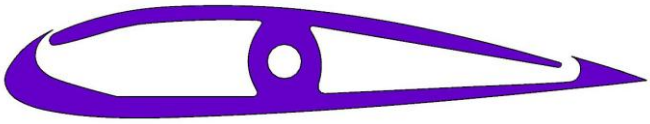

Fig 38: Side-view of the CFJ aerofoil

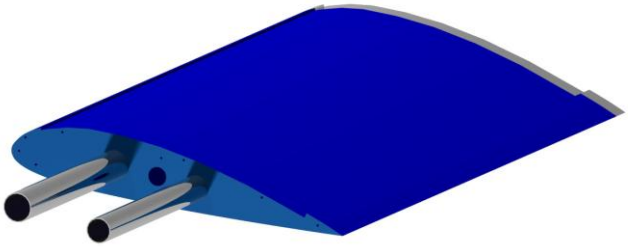

Fig 39: Air connection assembly

C. Materials and Machining

The initial CFJ wing was made from CNC (Computerized Numerical Control) routed MDF (Medium Density Fibreboard) wood panels. But due to structural considerations, the design was re-iterated and the model was built out of laser-cut acrylic sheets. Machined aluminium was used for the air connection tubing and manifolds.

Fig 40: Laser Cutting of Acrylic Sheets

D. Equipment

The experimental testing of the CFJ aerofoil required a number of equipment, which are explained in this section.

1. Wind Tunnel:

The experiment was conducted in a low-subsonic open circuit wind tunnel with a capacity to drive the free-stream air up to 50 m/s. The test section measures 1 m x 60 cm x 60 cm. The wind tunnel has provisions for mounting the test model. A circular plate was manufactured to support the compressor and vacuum tubes that project outside the test section.

2. Compressor and Vacuum pump

A Direct-driven Air Compressor supplies the pressurized air to the injection cavity. The details of the compressor are given (Table V).

Table V: Compressor specifications

Model:	MTX-8Ltr	Power:	7.5 HP
Displacement :	30 CFM	Pressure:	200 psi
Speed:	690 rpm	Weight:	24 kg
Voltage:	220 V	Tank:	80 gallons

A vacuum cleaner with a flow control attachment supplies vacuum pressure to the suction cavity.

Table VI: Port Locations

Port No	*X (mm)*	*x/c*	*Φ (deg)*
1	0.0	0.000	-90.000
2	1.5	0.005	-56.870
3	7.5	0.025	-46.600
4	26.0	0.087	-23.590
5	42.0	0.140	-15.060
6	71.0	0.237	-4.710
7	100.0	0.333	0.000
8	122.0	0.407	3.500
9	156.0	0.520	7.810
10	187.0	0.623	10.520
11	211.0	0.703	12.610
12	237.0	0.790	14.470
13	256.0	0.853	15.530
14	280.0	0.933	18.060
15	3.0	0.010	50.850
16	17.0	0.057	17.860
17	39.0	0.130	5.860
18	62.0	0.207	0.000
19	85.0	0.283	-1.990
20	108.0	0.360	-2.540
21	150.0	0.500	-3.840
22	184.0	0.613	-4.570
23	217.0	0.723	-5.320
24	246.0	0.820	-5.680

3. Instrumentation

Direct or indirect measurement of various flow variables was carried out to quantify information about the flow. The flow parameters to be measured were the free-stream velocity, static pressure over the aerofoil surface, velocity of the jet, mass flow rates at injection and suction, and injection and suction pressures. The measurement devices had to be both affordable and accurate to a certain extent. The following instruments were used to carry out flow measurements.

4. Pitot-static probe

The free-stream velocity was calculated from the differential pressure across the pitot and static pressure probes. The pitot and static probe arrangement were placed upstream of the test section, in order to have access to undisturbed free-stream air. The other end of the probe is connected to a multi-tube manometer. A separate pitot-static probe was used to obtain the pressures in the injection and suction cavity, and also to find the jet velocity at the point of injection.

5. Static ports on the aerofoil surface

A total of 24 static ports (14 on the aerofoil top surface, 10 on the bottom) were used to measure static pressures over the aerofoil surface. These included ports at the leading edge near the trailing edge, and at the injection and suction locations as well. These ports were installed at roughly one-third of the span, along the chord. The probes are

Retrieval Number: A10470581C19/19©BEIESP
Published By:
Blue Eyes Intelligence Engineering
& Sciences Publication

connected to a multi-tube manometer.

6. Multi-tube Manometer

The multi-tube manometer gives the pressure values at the ports of the pitot-static probes or the static probes directly in terms of water head. These values are processed to obtain the flow variables at the point of measurement.

7. Digital Anemometer

The velocities of the air at the compressor exit and the vacuum pump inlet was measured using the digital anemometer. These values were used to obtain the mas flow rate in the injection and suction cavities.

8. Port Locations

The static port locations and the corresponding angles are given (Table VI).

E. Results

The experimental C_p variation of the CFJ aerofoils for different AoAs are presented here.

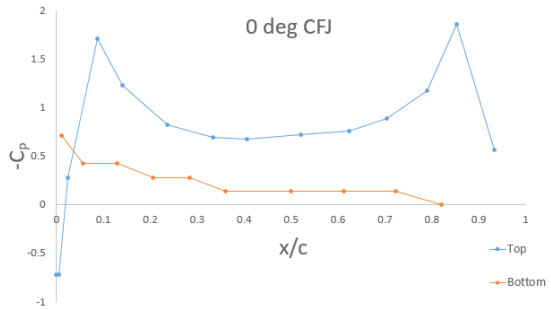

Fig 41: Cp variation for 0° AoA

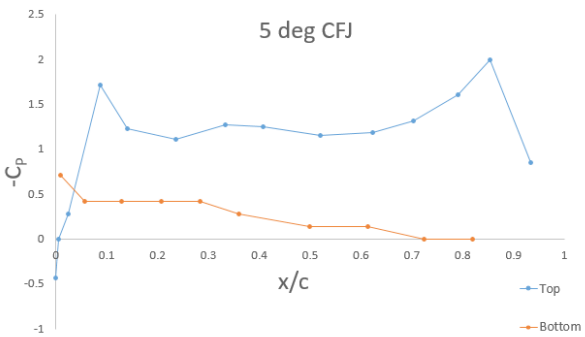

Fig 42: Cp variation for 5° AoA

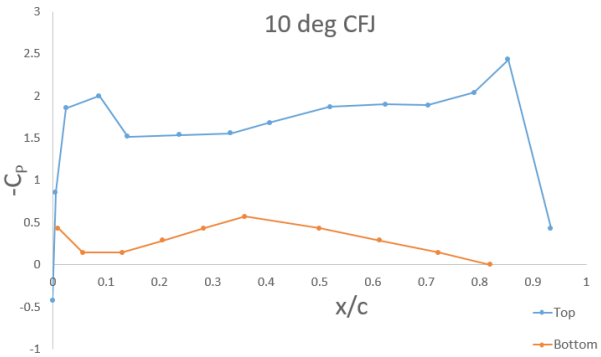

Fig 43: Cp variation for 10° AoA

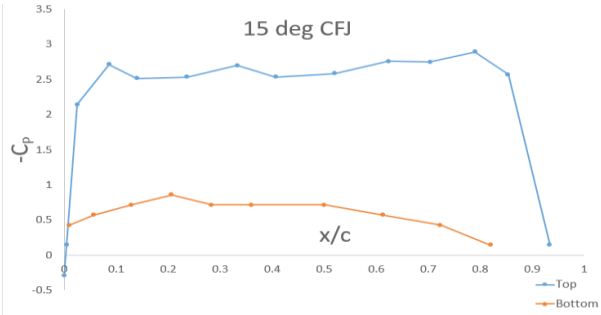

Fig 44: Cp variation for 15° AoA

The jet effects and the overall CFJ performance results are presented in this section. In addition to lift and drag created in the conventional way, the CFJ aerofoil generates jet effects from the reactant forces of the jet produced. A control volume analysis done on the CFJ aerofoil yields the following equations and these jet effects must be included in the calculation of overall lift and drag [29].

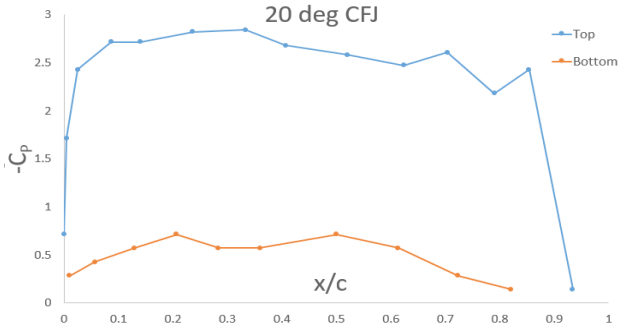

Fig 45: Cp variation for 20° AoA

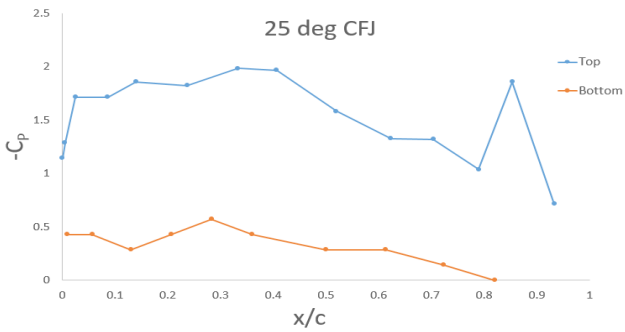

Fig 46: Cp variation for 25° AoA

$$F_x = (\dot{m}_j V_{j1} + p_{j1} A_{j1}) * cos(\theta_1 - \alpha) - \gamma(\dot{m}_j V_{j2} + p_{j2} A_{j2}) * cos(\theta_2 + \alpha) \quad (6)$$

$$F_y = (\dot{m}_j V_{j1} + p_{j1} A_{j1}) * sin(\theta_1 - \alpha) - \gamma(\dot{m}_j V_{j2} + p_{j2} A_{j2}) * sin(\theta_2 + \alpha) \quad (7)$$

Here subscript 1 indicates injection and 2 indicates suction. p_{j1} is the pressure in the injection cavity and p_{j2} is the static pressure in suction cavity. V_j is the velocity of the jet, A_j denotes the area of the jet. θ_1 and θ_2 are the angles formed by the injection and suction jet openings with the line

Retrieval Number: A10470581C19/19©BEIESP

Published By:
Blue Eyes Intelligence Engineering
& Sciences Publication

normal to the chord. For our aerofoil, θ_1 = 26.02°, θ_2 = 60.12°. The value of γ can be 0 or 1. It is 0 when there is no suction and only injection, and 1 when both injection and suction are used. The values of lift and drag are computed using the following equation.

$$L = R_y' - F_y \tag{8}$$

$$D = R_x' - F_x \tag{9}$$

Where, R_x' and R_y' are the surface pressure integrals along the free-stream and perpendicular to the free-stream respectively. The result summary is presented (Table VII).

Table VII: Summary of experimental results

$\alpha°$	F_x	F_y	R_x	R_y	C_L	C_D
0	0.705	-0.331	-0.289	7.519	0.711	-0.09
5	0.727	-0.33	0.308	10.755	1.005	-0.038
10	0.743	-0.33	2.052	14.617	1.355	0.119
15	0.753	-0.33	4.336	18.653	1.721	0.325
20	0.757	-0.33	6.717	18.615	1.718	0.44
25	0.756	-0.33	6.129	11.761	1.096	0.54

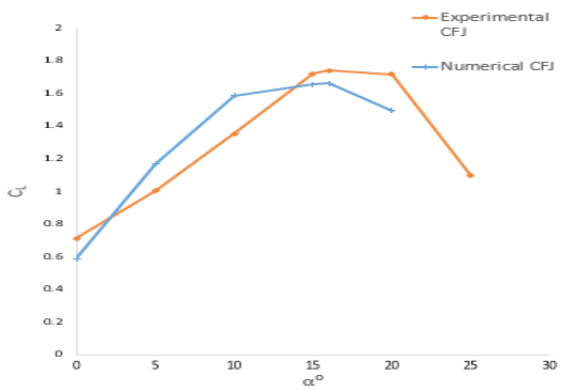

Fig 47: Lift and stall margin comparison

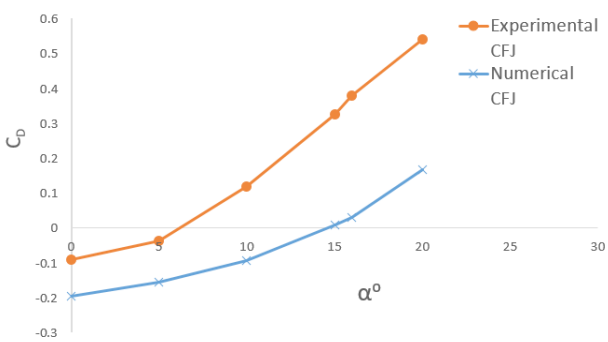

Fig 48: Drag comparison

The lift and stall margin result comparison are represented (Fig 47 – 48).

The experimental maximum lift coefficient (C_{Lmax} = 1.74) and numerical values are in good agreement with each other (4.5%) and the experimental stall angle is about 1 degree more than the stall angle obtained in numerical studies.

VII. CONCLUSION

The performance of a co-flow jet circulation technique was studied by applying the CFJ modification on a ClarkY-M18 aerofoil. The study was conducted at low speed (M=0.03) and low Reynold's Number (~200,000). The momentum coefficient was maintained at 0.05 throughout the study. Even at these primitive conditions, we observed an increase in C_{Lmax} of 37% and an increase in stall margin by 3 degrees (27% increase). The aerofoil was found to generate negative drag (thrust) at AoAs up to 15°.

A fair agreement was observed between the results of numerical studies and experimental results obtained for the CFJ ClarkY-M18-063-130 aerofoil at a Mach of 0.03. The trends of the variation of the flow properties were very similar in the experimental and the numerical case.

The co-flow jet is one of the most advanced flow control techniques available. The concept can be translated to a number of applications including short take-off aircrafts (STOL), Supermanoeuvrable aircrafts, long range commercial aircrafts, etc. Significant weight savings in terms of both structural weight and fuel weight can be achieved if this method is utilized correctly.

Further validation of the CFJ flow control method should include testing with higher energy jets and higher momentum coefficients. Studies on the effect of multiple injection and suction cavities should be performed in order to better understand this concept and make full utilization of the advantages this method provides. The discrete CFJ must be numerically analysed and experimentally validated. Studies must be conducted for other obstruction factors (OFs) and combinations of OFs for injection and suction. Experimental aircrafts that make use of the co-flow jet concept must be designed, fabricated and tested. These aircrafts can be small UAVs or MAVs. The methods of air delivery to and from the injection and suction slots must be improved and optimized. Also, other methods must be developed to decrease the strain on the engines while delivering the co-flow air. Lastly, studies must be performed on the effectiveness of CFJ when deployed along with flaps, slats and other FC techniques.

REFERENCES

1. G. Zha, "High Performance Aerofoil Using Co-Flow Jet Flow Control," (2005). AIAA Paper 2005-1260
2. Kirk, Danah, "Experimental and Numerical Investigations of a High Performance Co-Flow Jet Aerofoil" (2009). Open Access Theses. Paper 229
3. Md. Riajun Noor, "Effect of Co-Flow Jet over an Aerofoil: Numerical Approach," (2014). Khulna University of Engineering & Technology, Bangladesh
4. Lefebvre, Alexis Michel, "Investigation of Co-Flow Jet Flow Control and its Applications" (2015). Open Access Dissertations. Paper 1418.
5. Menter, F. R., "Zonal Two Equation k-ω Turbulence Models for Aerodynamic Flows", (1993). AIAA Paper 93-2906.
6. G. G. Stokes, "On the Effect of the Internal Friction of Fluids on the Motion of Pendulums," (1851). Transactions of the Cambridge Philosophical Society, vol. 9, pp.8106.

Retrieval Number: A10470581C19/19©BEIESP
Published By:
Blue Eyes Intelligence Engineering
& Sciences Publication

1. O. Reynolds, "An Experimental Investigation of the Circumstances which Determine Whether the Motion of Water Shall be Direct or Sinuous, and of the Law of Resistance in Parallel Channels," (1883). Philosophical Transactions of the Royal Society, vol. 174(0), pp. 935982.
2. L. Prandtl, "Königliche Gesellschaft der Wissenschaften zu Göttingen," (1918). ed. Tragflügeltheorie.
3. "With a View to Practical Solutions." http://history.nasa.gov/SP-4305/ch4.htm.Accessed: 2014-11-05.
4. L. Prandtl, "In Early Developments of Modern Aerodynamics," Butterworth Heinemann, Oxford, UK, p. 77, 2001. English Translation, Edited by J. A. K. Ackroyd, B. P. Axcell and A. I. Ruban.
5. "Human Flight." (2012) https://fugahumana.wordpress.com/2012/03/31/bio-mimeticdragreduction-part-2-aero-and-hydrodynamics/, Accessed: 2014-11-07.
6. B. L. Storms and C. S. Jang, "Lift Enhancement of an Aerofoil Using a Gurney Flap and Vortex Generators," (1994). Journal of Aircraft, vol. 31, no. 3, pp. 542–547.
7. R. Barrett and S. Farokhi, "On the Aerodynamics and Performance of Active Vortex Generators," (1993). AIAA 93-3447, 11th Applied Aerodynamics Conference,
8. "Nacelle Vortex Generator." http://www.aerospaceweb.org/question/aerodynamics/q0255.shtml. Accessed: 2014-11-06.
9. T. A. Harris and R. S. Swanson, "Wind-Tunnel Tests of an NACA 23021 AerofoilEquipped with a Slotted Extensible and Plain Extensible Flap," (1940). NACA TN 782.
10. T. A. Harris and I. G. Recant, "Wind-Tunnel Investigation of NACA 23012, 23021and 23030 Aerofoils Equipped with 40 Percent Chord Double Slotted Flaps." (1941). Report No. 723, NACA.
11. "High-Lift Systems." http://history.nasa.gov/SP-468/ch10-5.htm. Accessed: 2014-11-19.
12. J. A. Axelson, G. L. Stevens, "Investigation of a Slat in Several Different Positions on an NACA 64A010 Aerofoil for a Wide Range of Subsonic Mach Numbers." (1954). NACATN 3129.
13. H. L. Morgan, Jr., "Low-Speed Aerodynamic Performance of an Aspect-Ratio Supercritical-Wing Transport Model Equipped with a Full-Span Slat and Part-Span and Full-Span Double-Slotted Flaps." (1981). NASA-TP-1805.
14. O. Schrenk, "Experiments with Wbsaugefliigeln," (1935) Aviation Research, vol.12, p. 1027.
15. H. Schlichting, K. Gersten, "Boundary-Layer Theory," (2003) Springer, 8th Ed.
16. "Introduction to the Aerodynamics of Flight." http://history.nasa.gov/SP-367/chapt4.htm#f67. Accessed: 2014-11-19.
17. R. Barrett and S. Farokhi, "On the Aerodynamics and Performance of Active Vortex Generators," (1993) AIAA 93-3447, 11th Applied Aerodynamics Conference.
18. H. F. Muller-Vahl and D. Greenblatt, "Simulation of Active Flow Control on the Flap of a 2D High-Lift Configuration," (2015). AIAA Journal, vol. 53, pp. 277–295.
19. "PIV Analysis of Plasma Actuators." http://www.sppl.umd.edu/projects/13-pivanalysis.html. Accessed: 2015-03-26.227
20. M. L. Post and T. C. Corke, "Separation Control on High Angle of Attack Aerofoil Using Plasma Actuators," (2004) AIAA Journal, vol. 42, no. 11, pp. 2177–2184.
21. R. J. Englar, "Circulation Control Pneumatic Aerodynamics: Blown Force and Moment Augmentation and Modifications; Past, Present and Future." (2000) AIAA Paper 2000-2541.
22. L. W. Traub and M. Biegner, "Experimental Evaluation of a Self-Contained Circulation-Control Wing," (2013) Journal of Aircraft, vol. 50, no. 3, pp. 764–777.
23. G.-C. Zha, W. Gao, and C. Paxton, "Jet Effects on Co-Flow Jet Aerofoil Performance," (2007). AIAA Journal, No. 6, vol. 45, pp. 1222–1231.
24. G.-C. Zha and D. C. Paxton, "A Novel Flow Control Method for Aerofoil Performance Enhancement Using Co-Flow Jet." Applications of Circulation Control Technologies, Chapter 10, p. 293-314, Vol. 214.

AUTHORS PROFILE

Srinivasan S working as Assistant Professor at Department of Aerospace Engineering, RV College of Engineering, Bangalore, India, have pursued M. Tech in Aeronautical Engineering and have a teaching Experience of 12 years in Aerospace Engineering. Associate Life Member for Aeronautical Society of India.

Shreesha M is currently pursuing bachelor's degree in Aerospace Engineering at RV college of engineering. Research work- Two international publications and member of RnD in student Nano satellite team, Antariksh
Email: shreeshamadhu@gmail.com

Tanveer Ahmed is a student pursuing Bachelors in Aerospace Engineering at RV College of Engineering, Bengaluru, India - 560059. One international publication at 69th International Astronautical Congress 2018, Bremen. Head of Thermal Subsystem for RVSAT-1 and, a microbiological payload for PS4. Head of propulsion subsystem for Team Antariksh's sounding rocket. Strong ability to work on interdisciplinary projects and is experienced in multi role leadership (such as thermal control, propulsion, sponsorship and project management) in student projects. Area on interest include spacecraft propulsion and thermal control, fluids in space, aerodynamics, defence aircrafts, nonlinear analysis and aerospace project management.
Email: tanveertan98@gmail.com

G K Sanjana is a final year student at the Department of Aerospace Engineering, RV College of Engineering, Bangalore, India – 560059.
Email: sanjanagk.ae15@rvce.edu.in

Retrieval Number: A10470581C19/19©BEIESP

Published By:
Blue Eyes Intelligence Engineering
& Sciences Publication